Semiconductor Physics, Quantum Electronics & Optoelectronics, 2015. V. 18, N 3. P. 362-366.
doi: 10.15407/spqeo18.03.362

PACS 43.58.Bh, 71.20.Tk

Impedance anisotropy and quantum photocapacity of bio/inorganic clathrates InSe⟨histidine⟩ and gase⟨histidine⟩

F.O. Ivashchyshyn, I.I. Grygorchak, M.I. Klapchuk
Lviv Polytechnic National University, 12, S. Bandera str., 79013 Lviv, Ukraine
E-mail: Fivash@i.ua, Ivan_gryg@ukr.net, M.klapchuk@gmail.com

Abstract. Intercalated nanostructures of InSe⟨histidine⟩ and GaSe⟨histidine⟩ were formed. Phenomena of the negative capacitance and the quantum capacitance are visualized in the first nanostructure. The introduction of histidine between indium selenide layers leads to increasing of conductivity anisotropy ($\sigma_{\parallel}/\sigma_{\perp}$) from 67 to 226. Temperature dependences of the real component of the complex impedance indicate semiconductor mechanism of conductivity along nanolayers with two activation energies: 1.6 meV at low-temperature and 0.25 meV in high-temperature regions. Appearance of the giant high-frequency negative magnetoresistance and almost 20-fold photosensitivity increase are observed in the second nanostructure. The conductivity anisotropy of the nanostructure GaSe⟨htd⟩ ($\sigma_{\parallel}/\sigma_{\perp}$) is 10^2. Temperature dependence of the real component of complex impedance along the layers at temperature regions $-30 < t\,°C \le 10$, $10 < t\,°C \le 30$, $30 < t\,°C \le 50$ demonstrates cardinally different mechanisms of conductivity. Activation energies are 0.35 meV in the low-temperature and 0.69 meV in high-temperature intervals. Non-activated conductivity mechanism is observed within the range of temperatures $10 < t\,°C \le 30$. The parameters of the energy spectrum calculated using the Geballe-Pollak theory prior to and after introduction of histidine for two nanostructures are given; it well correlates with the experimental dates.

Keywords: InSe, GaSe, histidine, supramolecular structure, intercalation, impedance spectroscopy, Nyquist diagram.

Manuscript received 28.04.15; revised version received 29.07.15; accepted for publication 03.09.15; published online 30.09.15.

1. Introduction

With rapid development of nanoengineering (nanoelectronics, quantum coherent spinotronics, etc.) and with related to these sciences necessity to initiate creation of super-high capacitance accumulators of electric energy, formation of heterostructured inorganic-inorganic, inorganic-organic, and bio-organic materials attract still more attention of scientists. The ability to realize unique physical and chemical properties [1, 2], sometimes paradoxical, is associated with these materials.

The known methods of obtaining them, such as vacuum deposition, photolithography, synthetical Languir-Blodgett techniques, have some limitations caused by limited variability of the choice of different hetero-ingredients and by problematic synthesis of "host-guest" configuration, especially synthesis of heteroagregatic ones. By this time only a small experience gained on this way and made small steps [3, 4]. As far as bionanosemiconductor inorganic multilayered nanohybrids are concerned, nowadays, information on these investigations is lacking at all. Therefore, the aim of this work is to fill, to some extent, the gap in this branch of investigations.

2. Results and discussions

To form bio-inorganic/semiconductor nanohybrids, the layered crystals of gallium selenide (GaSe) and indium selenide (InSe) were used as semiconductor matrix and the aminoacid histidine ($C_6H_9N_3O_2$) was chosen as a biologically active guest element. The suggested three-stage scheme of nanoengineering of crystals was used in [5]. The main feature of histidine is that it is a zwitteron (i.e., it possesses properties of both anion and cation) with a colossal dipole moment.

Formation of the histidine nanolayers in a three-fold expanded matrix of indium selenide leads to more than forty-fold increasing the real component of specific complex impedance and to almost four-fold increasing the photosensitivity in the direction perpendicular to the plane of nanolayers.

At the same time, the effect of photoinduced "negative capacitance" is observed: the corresponding low-frequency impedance hodograph branch enters the fourth, inductive quadrant of the complex impedance plane, which correlates with the low-frequency oscillation Re Z(ω) under illumination (see curve *6* in Fig. 1). In this case, the mechanism of negative photocapacitance is most likely associated with the photoexcitation of electrons from occupied states below the Fermi level and, therefore, with formation of trap centers for injected electrons with the relaxation time longer than the half-period of a sinusoidal signal.

According to it, the equivalent electric circuit can be represented that shown in Fig. 2. The first parallel high-frequency link R_1//CPE_1 (where CPE_1 is element of constant phase capacitive type [6]) in the circuit models the distributed capacitance caused by the presence of vacancies or impurity defects that provide electronic conductivity at room temperature. Second R_2//CPE_2, the middle-frequency link, displays the path of current flow through energy barriers in guest positions. The low-frequency link C_Q//$R_{rec}L$ models the path current flow through the boundary of histidine/semiconductor matrix. Here, R_{rec} is the resistance recombination that simulates a barrier to charge C_Q, L – inductance, C_Q – quantum capacitance [7] that is described by the equation $C_Q = e^2 dn/dE_{Fn}$, where n is the concentration of electrons, E_{Fn} – energy of the electron Fermi quasi-level. For the latter branch of the low-frequency section, the admittance can be written as follows:

$$Y(\omega) = \frac{1}{R_{rec}} - i\,\omega C\,, \qquad (1)$$

where $C = C_L - C_Q$, $C_L = L/R_{rec}^2$.

According to equation (1), impedance of latter link in an equivalent electric circuit for an illuminated nanohybrid at very low frequencies $\left(\omega < \frac{1}{R_{rec}C}\right)$ is a parallel connection of the recombination resistance and constant negative capacitance C. Note that under condition $C_L > C_Q$ the low-frequency branch comes to the IV inductive quadrant, showing inductive response. Table 1 shows the parameters of the band spectrum prior to and after introduction of histidine in InSe, calculated using the Geballe-Pollak theory. It is evident that histidine encapsulation reduces the density of states at the Fermi level by an order of magnitude, which well correlates with low-frequency areas of Re Z(ω), at the same time, significantly reducing the distribution of trap centers. The radius of jump can be considered as a constant.

Research of the path current flow along the layers of expanded matrix InSe and nanohybridized structure InSe⟨htd⟩ within the frequency range (10^{-3}…1 Hz) showed that the conductivity anisotropy ($\sigma_{\parallel}/\sigma_{\perp}$) with introduction of histidine increases from 67 to 226.

The growth of Re Z(ω) perpendicular to the nanolayers after the introduction of histidine may be caused by decreasing of carrier mobility due to "rotational" polaron formation, and its falling along them likely caused by the increasing carrier concentration due to modification of the InSe band structure by electric field of "guest" assuming "ferroelectric" ordering of histidine dipoles along layers, as shown in Fig. 3a.

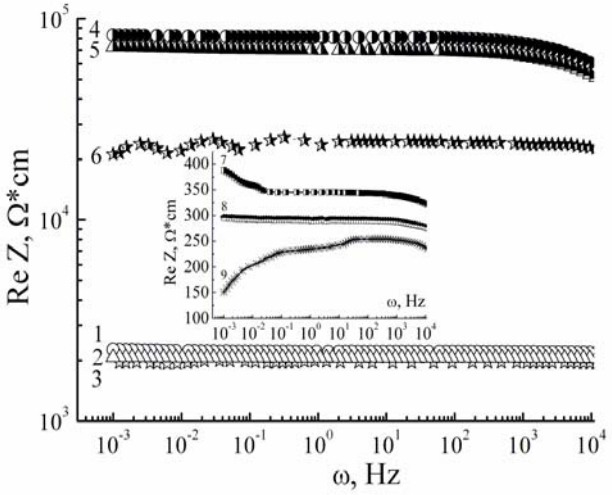

Fig. 1. Frequency dependences of complex impedance in perpendicular to the nanolayers of expanded matrix InSe (*1-3*) and of nanostructure InSe⟨htd⟩ (*4-6*), and along layers InSe⟨htd⟩ (*7-9*) measured in the dark (*1*, *4*, *7*), as well as under illumination (*3*, *6*, *9*), measured at the action of magnetic field (*2*, *5*, *8*).

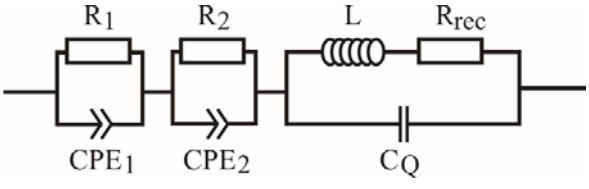

Fig. 2. The equivalent electric circuit.

Semiconductor Physics, Quantum Electronics & Optoelectronics, 2015. V. 18, N 3. P. 362-366.
doi: 10.15407/spqeo18.03.362

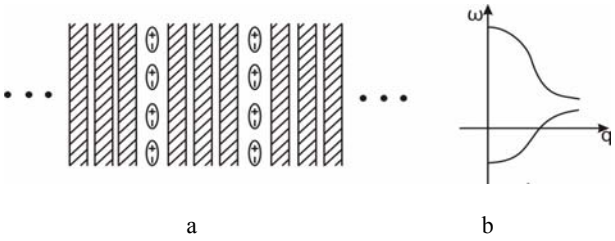

Fig. 3. Ferroelectric arrangement of dipoles (a) and the schematic presentation of band structure modification of InSe⟨htd⟩ layers (b).

As shown in our work [8], for the latter case along the *q*-axis of the Brillouin zone the valence band splits into two subbands, at the same time widths of subbands reduce comparatively to the unperturbed system.

A similar situation for the conduction band can be obtained. As a result, one of the branches of the valence band arises along the energy scale "up" and one of the branches of the conduction band goes "down" (Fig. 3b). As a consequence, the effective bandgap decreases, or conduction band catch the Fermi level, which leads to increasing of the concentration of carriers.

Photosensitivity along layers of InSe⟨htd⟩ is almost twice less than that in perpendicular to them, while for the expanded matrix these values are virtually identical. When illuminating, we observe an anomalous frequency dependence Re Z(ω): it is the monotonic growth with increasing frequency in fairly wide frequency range (curve *9* in Fig. 1). In this case, low-frequency branch of the impedance hodograph is almost parallel to Re Z axis with its opposite genesis ω, as well as to the relevant branch of hodograph built to measure in the dark. If the latter are modeled by finite element of constant phase (BCPE) [6], which reflects the path current flow in space-restricted area with the complex electrical conductivity, then under illumination one can propose a model of impedance along the layers containing the link with quantum capacity (Lurie [7]). In this case, it represents contribution from the histidine nanoclusters with the energy spectrum of the path current flow caused by the non-equilibrium carriers. As a result, the conductivity of non-equilibrium carriers due to gravity in accordance with the [9] should decrease with increasing the frequency, as observed in Fig. 1 (curve *3*).

Temperature dependences of the real component of the complex impedance along the layers (Fig. 4) indicate semiconductor nature of the electrical conductivity of nanohybrids with two activation energies: 1.6 meV in low-temperature and 0.25 meV in high-temperature regions. It is interesting to note that, for proper temperature, the change of conductivity mechanism at (–10 °C) corresponds to a radical change of the low-frequency branch in Nyquist diagrams: transfert to the fourth, inductive quadrant (inset to Fig. 4). It makes the base to assume that at temperatures higher than –10 °C captured by trap centers electrons would be delocalized. When reducing the temperature down to –30 °C, localized electrons are no longer delocalized in the tails of the density-of-states.

For the initial expanded matrix (curve *1* in Fig. 5), we have a usual situation: the corresponding hodograph of impedance is of two-arc form, and it represents the capacitive response of localized states and the frequency-dependent impedance proper caused by jumps between localized states near the Fermi level in the packet of atomic monolayers (high-frequency curve). The middle-frequency curve represents the path of current flow through widened spaces of actions of van der Waals forces. These arcs are modeled by means of BCPE, which represents the path of current flow in space-restricted domain of complex-valued electric conductance [10]. The low-frequency section represents distribution of active resistance element (caused by discretization of the energy spectrum of the expanded matrix of gallium selenide), this resistance is modeled by means of CPE with a low value of phase deviation $\zeta < 0.1$ [6].

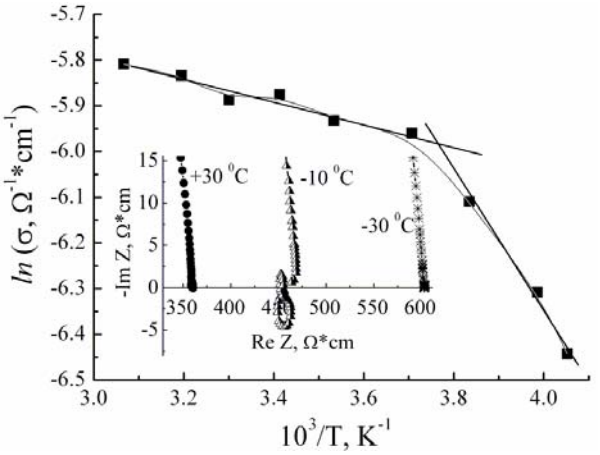

Fig. 4. Temperature dependences of the real component of impedance along nanolayers InSe⟨htd⟩. In the inset to Fig. 4 hodograph of impedance is given.

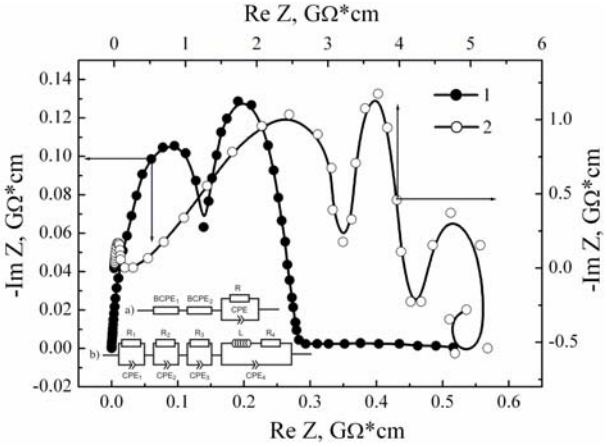

Fig 5. Nyquist diagram measured in the dark for the initial expanded matrix GaSe (*1*), and for the nanostructure GaSe⟨htd⟩ (*2*) and equivalent electric circuits corresponding to them.

Semiconductor Physics, Quantum Electronics & Optoelectronics, 2015. V. 18, N 3. P. 362-366.
doi: 10.15407/spqeo18.03.362

In this case, the equivalent electric circuit is given in the inset *a* to Fig. 5. Introduction of histidine leads to the increase in frequency dispersion of the impedance hodograph, and it indicates the emergence of additional potential barriers. Accordingly, the equivalent electric circuit is like to that shown in that inset *b* in Fig. 5. The latter link contains induction (inset *b* in Fig. 5) because the low-frequency branch of Nyquist diagram passes to the induction quadrant IV of the plane of complex-valued impedance. It indicates phenomenon of a "negative capacitance".

Introduction of histidine between selenide layers leads to twenty-fold growth of the real component of complex impedance in the low-frequency spectrum (10^{-3}…1 Hz) (Fig. 6). Lighting nanostructures GaSe⟨htd⟩ causes a decrease Re $Z(\omega)$ almost $5\cdot10^3$ times in the specified frequency range (curve *4* in Fig. 6). The latter phenomenon is quite expected, since this semiconductor matrix is photosensitive in the visible spectrum. However, compared to the enhanced matrix implementation histidine leads to an almost 20-fold increase in photosensitivity. At the same time, Fig. 6 (curve *4*) shows the previously non-observed effect of the giant high-frequency negative magnetoresistance: in the frequency range $60 < \omega \le 10^6$ Hz, the magnetic field 2.75 kOe at room temperature leads to a more than five-fold reduction of Re $Z(\omega)$. Taking into account no practical visualization of the magnetoresistance at lower frequencies this effect can most likely be associated with Zeeman delocalization of charge carriers from the deeper trap centers. Table 2 shows the parameters of the energy spectrum before and after introduction of histidine in GaSe, calculated using the Geballe-Pollak theory. In contrast to InSe, one can see a decrease of density of jumping centers and distribution of trap levels near the Fermi level.

Behavior of hodograph of impedance along the impedance layers GaSe⟨htd⟩ has the same character as in the measurement perpendicular, with the exception of the magnetic field. In this case, the frequency dispersion grows and middle/high-frequency branches of Nyquist diagrams "pass" to the inductive quadrant in the plane of complex-valued impedance (see the inset to Fig. 7). To some extent, it correlates with the above discussed Zeeman localization/delocalization of charge carriers.

Research of the current flow path along the layers of nanohybridized structure GaSe⟨htd⟩ showed that within the frequency range (10^{-3}…1 Hz) the electrical conductivity anisotropy is $\sigma_{\parallel}/\sigma_{\perp} \approx 10^2$, and reduction of the real component of the complex impedance under illumination reaches the ten-fold value. In contrast to the previous measurement geometry, in this case positive magnetoresistance is visualized at lower frequencies from 10^{-2} Hz: Re $Z(\omega)$ in a magnetic field is growing more than twice. In this case high-frequency negative magnetoresistance in the same frequency range not only preserved, but increasing reaches almost 14-fold value.

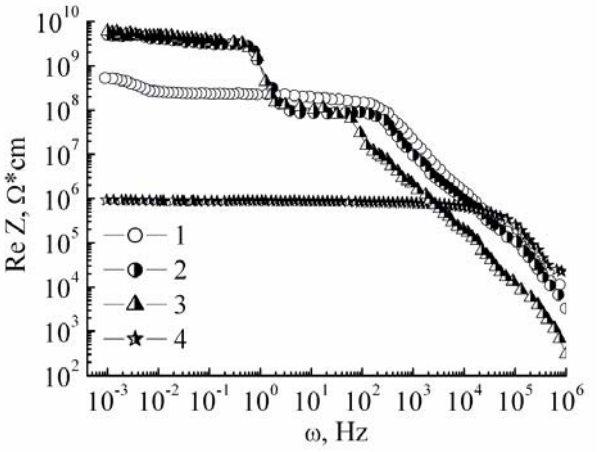

Fig. 6. Frequency dependences of the real component of impedance in perpendicular to the layers for initial expanded matrix GaSe measured in the dark (*1*) and for nanostructure GaSe⟨htd⟩ measured in the dark (*2*), as well as under illumination (*4*), measured at the action of magnetic field (*3*).

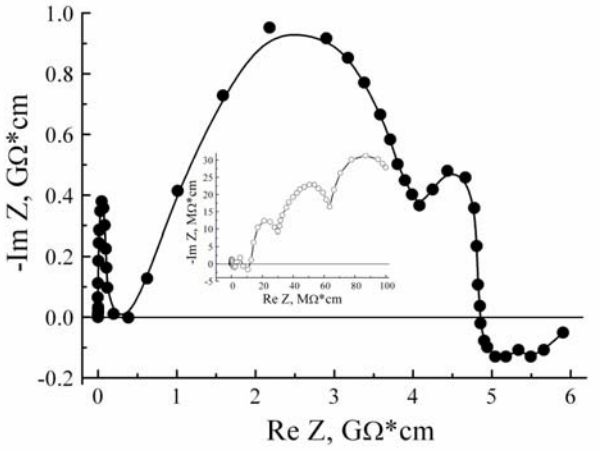

Fig. 7. Nyquist diagram GaSe⟨htd⟩ for the perpendicular to the layers and along them (see inset).

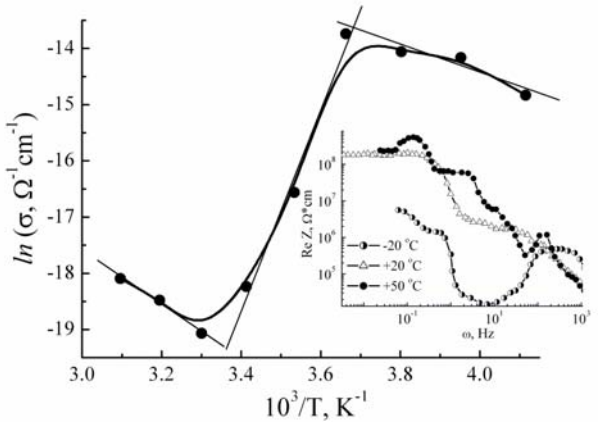

Fig. 8. Temperature dependences of the real component of impedance along nanolayers GaSe⟨htd⟩. On the inset, their frequency dependences are given.

Table 1. The parameters of the band spectrum prior to and after introduction of histidine in InSe.

	Density of jumping centers near the Fermi level, $N(F)\cdot10^{44}$, $J^{-1}m^{-1}$	Radius of jump $R\cdot10^{-8}$, m	The distribution of trap centers near the Fermi level, $J\cdot10^{-23}$, J	Real density of deep trap centers $N_t\cdot10^{22}$, m^{-3}
InSe	32.13	2.90	0.61	1.96
InSe⟨htd⟩	2.32	2.39	15.07	3.50

Table 2. The parameters of the energy spectrum prior to and after introduction of histidine in GaSe.

	Density of jumping centers near the Fermi level, $N(F)\cdot10^{43}$, $J^{-1}m^{-1}$	Radius of jump $R\cdot10^{-8}$, m	The distribution of trap centers near the Fermi level, $J\cdot10^{-22}$, J	Real density of deep trap centers $N_t\cdot10^{22}$, m^{-3}
GaSe	6.56	3.02	2.63	1.73
GaSe⟨htd⟩	10.60	2.83	1.99	2.10

Obviously, it is indicative of different energy structure in perpendicular and along the layers direction.

The temperature dependence of GaSe⟨htd⟩ along the layers demonstrates cardinally different mechanisms of conductivity within the temperature regions $-30 < t\ °C \leq 10$, $10 < t\ °C \leq 30$, $30 < t\ °C \leq 50$ (Fig. 8). If the first and last temperature ranges correspond to the activation mechanism, then one can obtain non-activation mechanism of conductivity within the range of temperatures $10 < t\ °C \leq 30$.

3. Conclusions

1. Introduction of histidine in the three-fold expanded matrix of indium selenide leads to the forty-fold increase of a real component of specific complex impedance and almost four-fold increase in photosensitivity in the direction perpendicular to nanolayers.
2. Appearance of photoinductive "negative photo-capacitance" is observed for nanostructure InSe⟨htd⟩; the mechanism of this phenomenon is a most likely associated with the photoexcitation of electrons from occupied states below the Fermi level and, therefore, with formation of trap centers for injected electrons with the relaxation time greater than the half-period of the sinusoidal signal.
3. The conductivity anisotropy ($\sigma_{\parallel}/\sigma_{\perp}$) due to introduction of histidine in extended matrix of InSe⟨htd⟩ increases from 67 to 226 within the frequency range (10^{-3}…1 Hz).
4. Temperature dependence of a conductivity of nanostructure InSe⟨htd⟩ has a semiconductor character with two activation energies 1.6 and 0.25 meV.
5. The introduction of histidine in three-fold expanded matrix of gallium selenide leads to the twenty-fold increase of a real component of specific complex impedance and the twenty-fold one for photosensitivity in the direction perpendicular to nanolayers.
6. The evidence of a giant high-frequency negative magnetoresistance is obtained for the nanostructure GaSe⟨htd⟩ in the constant magnetic field 2.75 kOe at room temperature; magnetic field leads to a more than 5-fold reduction of $\mathrm{Re}\,Z(\omega)$ within the frequency range $60 < \omega \leq 10^6$ Hz.
7. The conductivity anisotropy ($\sigma_{\parallel}/\sigma_{\perp}$) for the nanostructure GaSe⟨htd⟩ is 10^2, and decrease of a real component of the complex impedance under illumination reaches the ten-fold value. At the same time, positive magnetoresistance is visualized at frequencies less than 10^{-2} Hz: $\mathrm{Re}\,Z(\omega)$ growth more than twice in magnetic field, and high-frequency negative magnetoresistance growth reaching almost 14-fold value.

References

1. J.H. Choy, S.J. Kwon, G.S. Park // *Science*, **280**, p. 1589 (1998).
2. J.H. Choy, S.Y. Kwak, J.S. Park, Y.J. Jeong et al. // *J. Am. Chem. Soc.* **121**, p. 1399 (1999).
3. I. Grygorchak, F. Ivashchyshyn, P. Stakhira et al. // *J. Nanoelectron. Optoelectron.* **8**(3), p. 292 (2013).
4. T.M. Bishchaniuk, I.I. Grygorchak // *Appl. Phys. Lett.* **104**, p. 203104-1 (2014).
5. F. Ivashchyshyn, I. Grygorchak, P. Stakhira et al. // *J. Exper. Nanosci.* **9**(7), p. 678 (2014).
6. Z.B. Stoinov, B.M. Grafov, B. Savova-Stoinova, V.V. Yelkin, *Electrochemical Impedance.* Moscow, Nauka, 1991 (in Russian).
7. S. Luryi // *Appl. Phys. Lett*. **52**(6), p. 501 (1988).
8. F. Ivashchyshyn, I. Grygorchak, O. Sudakova et al. // *Mater. Sci. & Technol.* **27**(11), p. 973-978 (2011).
9. V.L. Bonch-Bruyevich, S.G. Kalashnikov, *Semiconductor Physics*. Moscow, Nauka, 1977 (in Russian).
10. *Impedance Spectroscopy. Theory, Experiment and Application.* Eds. E. Barsoukov, J.R. Macdonald. Wiley Intersci., Canada, 2005.